

The Catalytic Copper Clusters of the Particulate Methane Monooxygenase from Methanotrophic Bacteria: Electron Paramagnetic Resonance Spectral Simulations

Shao-Ching Hung^a (洪紹菁), Chang-Li Chen^b (陳昌立), Kelvin H.-C. Chen^b (陳皇州),
Steve S.-F. Yu^b (俞聖法) and Sunney I. Chan^{a,b*} (陳長謙)

^aA.A. Noyes Laboratory of Chemical Physics, 127-72 California Institute of Technology,
Pasadena, California 91125, USA

^bInstitute of Chemistry, Academia Sinica, Nangang, Taipei 115, Taiwan, R.O.C.

The particulate methane monooxygenase (pMMO) from *Methylococcus capsulatus* contains 14-15 reduced copper ions, and it has been proposed that these copper ions are arranged in the form of trinuclear clusters. Two of these clusters have been referred to as catalytic clusters (C-clusters) and have been implicated in dioxygen activation and alkane hydroxylation. The remaining copper ions appear to provide a “reservoir” of reducing equivalents to replenish the electrons at the C-clusters following dioxygen activation at the C-clusters during turnover. Accordingly, they are normally reduced and have been called electron-transfer clusters (E-clusters). For pMMO prepared in highly enriched membranes, or purified as the pMMO-detergent complex from these membranes, only the C-cluster copper ions are oxidized. Recently, the low temperature EPR spectrum of as-isolated pMMO was deconvoluted into a type 2 Cu(II) signal and a broad, but nearly isotropic EPR signal centered at $g \sim 2.1$. Earlier magnetization and magnetic susceptibility measurements have suggested that the latter EPR signal, which is not sensitive to microwave power saturation, might arise from a ferromagnetically exchange-coupled trinuclear Cu(II) cluster with $J \approx 20 \text{ cm}^{-1}$ and $D \leq 0.05 \text{ cm}^{-1}$. Toward confirming these results, several triangular model Cu(II) complexes, both antiferromagnetically and ferromagnetically coupled and with well-defined structural and ligand information, were reviewed to gain insights into magneto-structural correlations. Spectral simulations of the pMMO cluster EPR signals were then performed based on the structural and spectroscopic information provided by the ferromagnetic model complexes. We show that only Cu(II) ions with proper g -tensors and appropriate relative orientations between them can give rise to the unique EPR signal observed for the C-cluster(s) in pMMO. The putative C-cluster EPR signal observed for the as-isolated pMMO at 3 K was best fitted by a triad of ferromagnetically coupled Cu(II) ions with the following sets of g -values: (1.983, 2.030, 2.218), (1.983, 2.029, 2.218) and (2.000, 2.033, 2.207); and zero-field splitting parameters $D = 0.017 \pm 0.002 \text{ cm}^{-1}$ ($175 \pm 25 \text{ Gauss}$) and $E/D = 0.15$. The fit was not sensitive to the value of J so long as the exchange interaction was much larger than the Zeeman interaction ($J \gg g\beta H$).

Keywords: Electron paramagnetic resonance; Ferromagnetic exchange coupling; Monooxygenases; Oxidases; Spectral simulations; Trinuclear copper clusters.

INTRODUCTION

Many multi-copper-containing oxidases and monooxygenases are known in nature. The best characterized oxidases include laccase,¹⁻⁴ ceruloplasmin,⁵ and ascorbate oxidase,^{6,7} where the x-ray structures have been determined and a good deal of information is known about structure and function. In each of these oxidases, the oxidation of an organic substrate is linked to the reduction of dioxygen. The latter chemistry

involves a cluster of three reduced copper ions, although other copper ions, particularly blue copper(s), are often also involved in shuttling reducing equivalents from the substrate to the trinuclear copper cluster(s). Among the monooxygenases, tyrosinase is perhaps the best understood.⁸ Other multi-copper monooxygenases include β -dopamine monooxygenase⁹ and the copper based peptidyl monooxygenase.¹⁰ The active site in tyrosinase involves only a pair of reduced copper ions, which not only activates molecular oxygen but also me-

Dedicated to Professor Sunney I. Chan on the occasion of his 67th birthday and his retirement from professional life.

* Corresponding author. E-mail: chans@chem.sinica.edu.tw

diates the ultimate transfer of one of the oxygen atoms to the tyrosine substrate to form the catechol at the catalytic center. Recently, similar chemistry has also been suggested at the catalytic site of the membrane-bound (particulate) methane monoxygenase (pMMO).¹¹⁻¹⁵ Here, a pair of reduced trinuclear copper clusters are implicated. In fact, the dioxygen chemistry in pMMO appears to mimic that of the multi-copper oxidases, whereas the oxo-transfer chemistry mimics that of tyrosinase.

Although all of the above oxidases and the pMMO seem to involve trinuclear copper clusters in the activation of dioxygen at the active site, the details of the chemistry mediated appear to be very different. In the case of the oxidases, the copper cluster catalyzes the conversion of dioxygen to two water molecules. In the case of pMMO, two trinuclear copper clusters are apparently involved.¹⁶ One of the copper clusters catalyzes the oxo-transfer to a C-H bond and the reduction of the second oxygen atom in the presence of protons to form a water molecule. The other copper cluster appears to mediate dioxygen chemistry only, with the fourth electron required originating apparently from the C-cluster where the alkane hydroxylation occurs. Apparently, the structural details of the trinuclear copper clusters among the various proteins are also not the same. The catalytic sites in the case of pMMO appear to involve fairly symmetrical trinuclear Cu(I) clusters.¹¹⁻¹³ In the case of the multi-copper oxidases, the structure of the copper cluster is asymmetric, with a reduced type 2 copper site in close proximity to a reduced type 3 binuclear copper site.⁶⁻⁸ In other words, the geometrical disposition of the three copper ions is intrinsically different at the active site(s) between the two types of enzymes.

It has been proposed that when the trinuclear copper clusters of pMMO are fully oxidized, each of the oxidized clusters consists of three type 2 copper centers that are mutually weakly ferromagnetically coupled.¹¹ Evidence in partial support of this picture for at least one of the C-clusters has recently been derived from analysis of the low temperature EPR of the as-isolated pMMO, when the enzyme is isolated and re-oxidized in air but without the hydrocarbon co-substrate.¹⁶ In contrast, when the copper ions in the corresponding clusters of laccase, ascorbate oxidase, or ceruloplasmin are oxidized, one observes a type 2 Cu(II) site that is at most weakly coupled to a pair of type 3 copper ions that are strongly antiferromagnetically coupled through a bridging hydroxyl ligand.⁸ While these differences in the electrostatic properties of the clusters no doubt reflect the different structural arrangements of the copper ions in the clusters, the detailed ligand structures of the copper ions in the clusters most cer-

tainly account for variations in the catalytic activity.

Electron paramagnetic resonance (EPR) spectroscopy has proven to be one of the most powerful tools in classifying the various copper sites in multi-copper oxidases, and similarly, EPR is proving to be useful in defining the various copper sites in pMMO. Unfortunately, in the case of pMMO, there are far too many copper ions, and they all seem to be grouped into trinuclear clusters of rather similar structures. Accordingly, in the fully oxidized enzyme, the EPR spectrum of the copper ions is a composite of heterogeneous contributions from several trinuclear copper clusters at the same time. While this general picture has been confirmed by magnetic susceptibility measurements on the fully oxidized protein,¹¹ a detailed characterization of the individual clusters has remained untractable. It is possible to make some limited progress toward this problem by exploiting the differential reactivity of the C-clusters and E-clusters toward dioxygen (and to NO).¹² The E-cluster copper ions remained reduced under these conditions so that the reaction products formed at the C-clusters could be followed and characterized by EPR. Nevertheless, further insights could be derived from the EPR if the correlation of the motions of the spins associated with the copper ions in the oxidized clusters could be better understood in structural and electronic terms.

This paper focuses on the EPR of one of the C-clusters in the pMMO, namely the one that is typically observed in the as-isolated form of the enzyme.^{16,17} Since the biological activity of pMMO is rather unique, and there is certainly no precedent for the EPR spectrum that we have observed for the oxidized pMMO copper clusters in metalloenzymes, we have decided to appeal to model compounds of trinuclear Cu(II) clusters with well-defined ligand structures and geometry that have already been reported in the literature. Specifically, we compare the EPR spectra observed for one of the C-clusters of pMMO with those of model trinuclear Cu(II) clusters and use this exercise to derive some insights into the possible ligand structures present within the trinuclear copper clusters in pMMO. We shall fine-tune the spin Hamiltonian parameters for the copper ions in these clusters via computer simulations to fit the 3 K and 77 K spectra recently recorded for the putative C-cluster in the as-isolated protein.¹⁶

MATERIALS AND METHODS

pMMO-Enriched Membranes from *Methylococcus capsulatus* (Bath)

The pMMO enriched-membranes were isolated and pu-

rified from cells of *Methylococcus capsulatus* (Bath) that were grown under NMS buffer (ATCC medium: 1306 nitrate mineral salts medium) at 30 μM CuSO_4 on a Bioflo 3000 fermentor (New Brunswick Inc.) equipped with a 5-L fermentor vessel, and adapted with a hollow-fiber reactor that allows precise control of the copper ion concentration in the culture media, as described in a recent publication from this laboratory.¹⁷ The membranes were typically 80% enriched in the pMMO, and were suspended in 25 mM PIPES buffer (pH 7.4). The average copper content in the pMMO was 13-14 moles of copper/mole of protein, assuming that the pMMO hydroxylase is a monomer with a subunit composition of $\alpha\beta\gamma$ of molecular mass 99 kDa.¹⁷ The pMMO in these membranes exhibited a specific activity of 60-80 nmol propylene oxide/min/mg protein when assayed using NADH as the reductant.

EPR Spectroscopy

EPR spectra were obtained at X-band (9.49 GHz) by using a Bruker E500 spectrometer equipped with a Bruker TE102 cavity. During EPR experiments, the sample temperature was maintained at 77 K by immersion of the EPR tube in a liquid-nitrogen containing finger dewar, or 3 K by using an Oxford Instruments continuous liquid-helium cryostat equipped with a helium pump to lower the vapor pressure of the liquid helium. A 500 μM of CuSO_4 in a 1:1 v/v water/glycerol mixture was employed as a standard sample for spin counting purposes. EPR spectra of the background were also recorded prior to double integration to determine the Cu(II) concentration in the sample.

THEORETICAL TREATMENT

Cluster models

The chemistry of trinuclear Cu(II) complexes has drawn considerable interest following their identification as the active sites of oxidases and oxygenases.^{1-8,11,12,14} Over the years, however, there has also been much interest in these complexes for the development of new inorganic materials showing molecular ferromagnetism.¹⁸⁻²⁰ Thus, many triangular Cu_3 complexes have been reported.²¹⁻⁴² Examples of some equilateral triangular copper clusters are shown in Fig. 1. Depending on the coordination geometry of the copper ions in the clusters and the degree of potential "overlap" of the d-orbitals containing the unpaired electron spins, these complexes exhibit varying degrees of exchange interactions, both antiferromagnetic and ferromagnetic. Thus, the model complexes **1**^{22,23} and **2**^{26,27} in Fig. 1 exhibit antiferromagnetic in-

teractions among the Cu(II) ions, whereas complexes **3** and **4** show ferromagnetic interactions.^{36,40} In **1** and **2**, the Cu(II) ions adopt square pyramidal coordination with the $(d_{x^2-y^2})^1$ ground "hole" states. The strong antiferromagnetic interaction ($J = -61$ to -500 cm^{-1}) in **1** is due to the effective overlap of the magnetic $d_{x^2-y^2}$ orbitals arising from the co-planarity of the coordination planes of the three subunits. Compound **2** displays a much weaker magnetic interaction ($J = -12$ to -15 cm^{-1}) than **1**. In **2**, bridging O atoms coordinate pairs of penta-coordinated copper atoms in an axial-equatorial arrangement, and a central O (or OH) bridge constrains the coordination planes to be orthogonal to each other. Thus, the overlap of the magnetic orbitals, either through the pair-wise bridging O ligands or the central O bridge, is weaker.^{26,27} It is evident that the magnitude of the magnetic coupling in these triangular Cu(II) complexes strongly depends on the overall degree of co-planarity of the ligand frameworks associated with each of the copper ions.

Compound **3** belongs to the class of trinuclear Cu(II) clusters where a carbonate anion serves as a tridentate bridge.³⁹⁻⁴² Here, the coordination environment of each copper ion is also square pyramidal so that each copper ion has the $(d_{x^2-y^2})^1$ ground "hole" states, as those in **1** and **2** (squares are drawn by dashed line in Fig. 1). However, the interaction among the Cu(II) ions is weakly ferromagnetic, and the com-

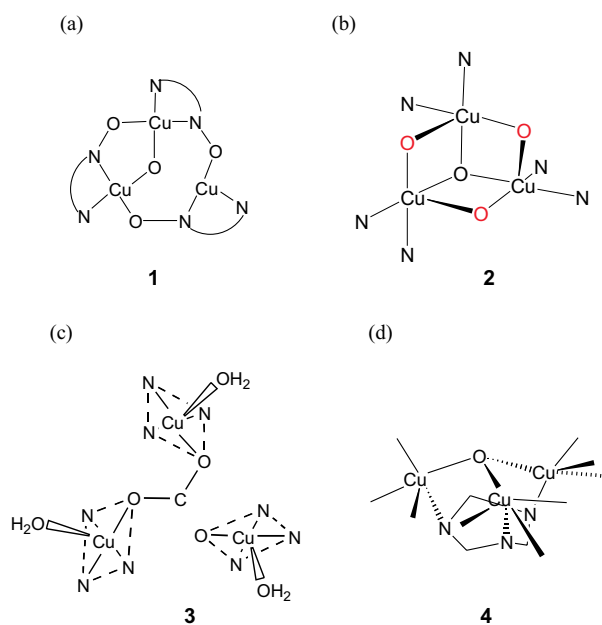


Fig. 1. Molecular structures of equilateral triangular Cu(II) clusters (a) taken from reference 23; (b) taken from reference 26; (c) taken from reference 40; and (d) taken from reference 36.

plex exhibits a $S = 3/2$ quartet ground state, similar to that proposed for the C-clusters in pMMO. According to Kahn,⁴³ the exchange coupling constant J can be expressed as a sum of both ferromagnetic (J_F) and antiferromagnetic (J_{AF}) contributions; i.e., $J = J_F + J_{AF}$. Both the antiferromagnetic and ferromagnetic contributions become attenuated when the metal ions are bridged by extended polyatomic ligands. However, the antiferromagnetic contribution is typically only important when there is direct overlap between the magnetic orbitals centered on nearest-neighbor metal ions, where it is then proportional to the square of the overlap integral between magnetic orbitals. In **1** and **2**, the exchange coupling is provided by a single bridging O, and the Cu-O-Cu pathway offers efficient overlap of magnetic orbitals on adjacent Cu(II) ions to mediate a strong antiferromagnetic exchange interaction. In **3**, the *syn-anti* arrangement of the O atoms in the carboxylate anion predisposes the 2p-orbitals of the oxygen atoms on the bridging carboxylate to an unfavorable overlap.⁴⁰ In addition, the CuN₃O planes are tilted with respect to the practically planar CO₃Cu₃ fragment by an average dihedral angle of 61.5° so that the equatorial planes of adjacent copper ions form average dihedral angles of 80.9°. This non-co-planarity is expected to decrease the overlap of the magnetic orbitals in the bridging region further and to lower the antiferromagnetic interaction. Accordingly, the ferromagnetic contribution becomes more dominant ($J = 6$ to 8 cm⁻¹), as revealed by magnetic susceptibility measurements.

On the other hand, the ligand geometry of each Cu(II) ion in compound **4** is best described as a distorted trigonal bipyramid, which leads to a d_{z^2} ground "hole" state.³⁶ The Cu-O-Cu angles in this complex (112°-113°) are also larger compared to those of the other two complexes. A fairly strong ferromagnetic interaction ($J = 54.5$ cm⁻¹) among the copper ions in compound **4** was concluded from magnetic susceptibility measurements. However, an analysis of the super-exchange pathway(s) that might lead to the observed ferromagnetic coupling among the copper ions is not straightforward.

Trinuclear Cu(II) complexes exist also as isosceles triangular complexes. Most show the doublet ground state, and only one complex has been shown to exhibit the quartet ground state. Fig. 2 shows two examples of such model complexes. Complex **5** exhibits a total spin $S = 1/2$ for the ground state,²⁹ while complex **6** has a quartet ground state.^{32,44} In both complexes the environment around the Cu(II) ions is distorted square pyramidal so that the magnetic orbitals centered on the Cu(II) ions have predominantly $d_{x^2-y^2}$ character.

In the case of complex **5**, the observed strong antiferromagnetic coupling ($J = -448$ cm⁻¹) could be accounted for in terms of a super-exchange mechanism operating via the Cu-N₂O₂-Cu linkage. However, such bridging networks are not co-planar, which should diminish the overlap between the magnetic orbitals. Thus, the unusually large spin exchange interaction in this complex was suggested to involve the electronic structure of the bridging ligand with a σ -orbital exchange pathway, which is independent of the angles between the basal planes of Cu(II) ions. On the other hand, the non-co-planarity of the mixed-bridge system in complex **6** results in a ferromagnetic exchange interaction of ~ 26 cm⁻¹ between the central and terminal Cu(II) ions, while the exchange coupling constant between the terminal copper ions is ~ 0 cm⁻¹. Based on the results of a SCF-CI calculation of a dimeric model molecule constructed from the crystal structure of **6**, the exchange coupling changes from antiferromagnetic to ferromagnetic exchange coupling as the dihedral angle between the basal planes of central and terminal Cu(II) increases, i.e., from co-planar structure to folded structure. Similar results have also been obtained in a study of the ferromagnetism of binuclear copper clusters with small Cu-O-Cu angles ($< 97.5^\circ$). Therefore, the magneto-structural correlation of polynuclear copper clusters could be understood in terms of the exchange interactions of their binuclear building blocks, which are already quite well established experimentally and theoretically.⁴⁵

A cluster model for the C-clusters of pMMO

Of the various cluster models discussed in the previous section, complex **6** probably offers the most likely comparison to the C-clusters in pMMO, particularly given the ligand types that are available for the copper ions in a protein environment. Nevertheless, we have undertaken EPR simulations on two of the ferromagnetically exchange-coupled trinuclear

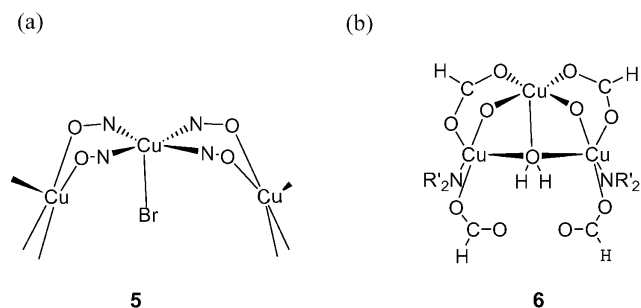


Fig. 2. Structures of isosceles triangular Cu(II) model complexes (a) taken from reference 29; and (b) taken from reference 32.

Cu(II) model complexes highlighted in the previous section, namely **3** in addition to **6**, to allow comparisons with the experimentally EPR spectra reported for these complexes. Although no EPR spectrum has been reported for complex **4**, we have considered both the trigonal bipyramidal coordination of the Cu(II) ions in complex **4** as well as the square pyramidal coordination in complex **3** and **6**, in order to ascertain the effects of local coordination geometry on the EPR spectrum.

Obviously, in each case, the observed g values and directions must refer to the individual g -tensors of the three copper ions in the complex. The relative orientation between the g -tensors of the Cu(II) ions as well as the strength of the ferromagnetic interactions vary with the geometrical disposition and the coordination geometry of the Cu(II) ions. The g -tensor orientation of individual Cu(II) ions for **3**, **4**, and **6** are depicted in Fig. 3(a), (b), and (c), respectively. In each case, the principal axes of the local coordinate system for the individual Cu(II) ions are labeled as x^* , y^* , and z^* for the g -tensor. For either square pyramidal coordination in **3** and **6** or trigonal bipyramidal coordination in **4**, the equatorial plane defines the x^* - y^* plane, whereas the z^* axis lies along the apical (axial) direction. Although distortions from ideal coordination geometry might occur, these distortions will be neglected and the g -tensors are assumed to align with the idealized geometry.

EPR simulations

The spin Hamiltonian appropriate to describe the three interacting paramagnetic copper ions within a trinuclear Cu(II) complex can be written as the sum of the spin Hamiltonians for the individual spin centers and the spin Hamiltonian describing the exchange interaction (eq 1):

$$\begin{aligned}
 H = & \beta_e \cdot \mathbf{B} \cdot \mathbf{g}_A \cdot \mathbf{S}_A + \beta_e \cdot \mathbf{B} \cdot \mathbf{g}_B \cdot \mathbf{S}_B + \beta_e \cdot \mathbf{B} \cdot \mathbf{g}_C \cdot \mathbf{S}_C \\
 & - 2 \cdot J_{AB} \cdot \mathbf{S}_A \cdot \mathbf{S}_B - 2 \cdot J_{BC} \cdot \mathbf{S}_B \cdot \mathbf{S}_C - 2 \cdot J_{CA} \cdot \mathbf{S}_C \cdot \mathbf{S}_A \\
 & + \mathbf{S}_A \cdot \mathbf{D}_{AB} \cdot \mathbf{S}_B + \mathbf{S}_B \cdot \mathbf{D}_{BC} \cdot \mathbf{S}_C + \mathbf{S}_C \cdot \mathbf{D}_{CA} \cdot \mathbf{S}_A
 \end{aligned}
 \quad (1)$$

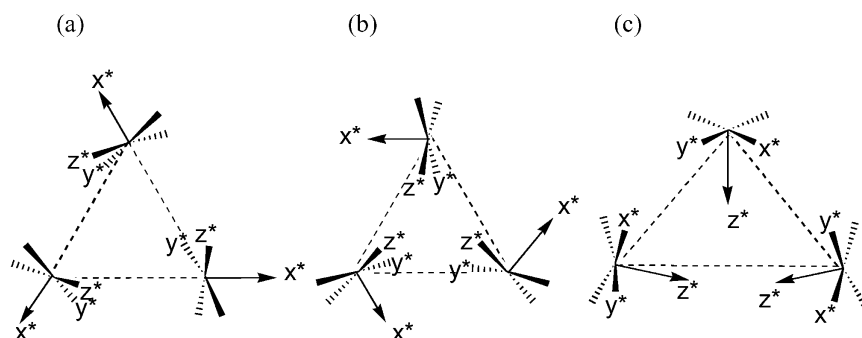


Fig. 3. The orientations of the local g -tensors for compounds **3**, **4**, and **6**, ((a), (b), and (c), respectively).

Here, the three Cu(II) ions are labeled as A, B, and C, respectively. \mathbf{g}_i , J_{ij} , and \mathbf{D}_{ij} denote the Zeeman g -tensor of spin centers i ; the isotropic (or scalar) exchange interaction between interacting centers i and j ; and the zero field splitting tensor (anisotropic part of the exchange and the dipolar interactions) between the interacting spin centers i and j , respectively. For the trinuclear Cu(II) complex, each Cu(II) ion has $S = 1/2$. The overall zero-field splitting is taken into account when the total electron spin S_T is ≥ 1 . \mathbf{D} will be used to describe the anisotropic part of the overall exchange interactions and the magnetic dipole-dipole interactions. Normally, two energy parameters, D and E , representing the axial and rhombic parameters, respectively, are used to describe the overall zero-field splitting. The D value refers to $3/2$ of the D_{\parallel} or D_{zz} component in the D -tensor, and E is defined as $(D_{\perp} - D_{\perp'})/2$, or $(D_{xx} - D_{yy})/2$. Here, x , y , and z denote the principal axes of the D tensor in the plane and perpendicular to the triangular plane.

Each Cu(II) ion in the trinuclear cluster can be represented by a g -tensor. The principal axes of the universal reference frame throughout the course of the present study are shown in Fig. 4(a). The local g -tensors are not necessarily di-

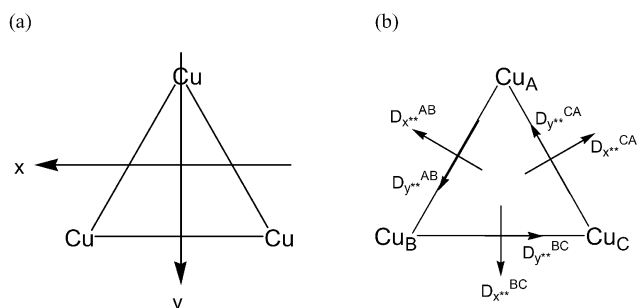


Fig. 4. (a) Principal axes of the universal coordination system used in the EPR simulations. (b) Relative orientation of the D -tensors for each interacting Cu(II) pair in the trinuclear Cu(II) cluster complexes.

agonal in this reference frame, but they are diagonal in their local coordinate systems (see Fig. 3). Therefore, these local g-tensors have to be transformed to the reference frame.

It is well known that the g-tensor of exchange-coupled systems ($\tilde{g}_{S,SAB}$) can be expressed as a linear combination of the local g-tensors.⁴⁶ For symmetric triads of $S = 1/2$ centers, the relations of the g-tensors are given below:

$$\begin{aligned}\tilde{g}_{3/2,1} &= 1/3 (\tilde{g}_A + \tilde{g}_B + \tilde{g}_C), \\ \tilde{g}_{1/2,1} &= -1/3 \tilde{g}_A + 2/3 \tilde{g}_B + 2/3 \tilde{g}_C, \\ \tilde{g}_{1/2,0} &= \tilde{g}_A.\end{aligned}\quad (2)$$

In the case of the zero-field splitting, the major contributions are from the spin-orbit couplings and the magnetic dipolar interactions between adjacent copper ions. Thus, the principal axes of the D-tensor of each interacting pair in the trinuclear cluster cannot be explicitly determined. In the present study, the relative orientation of the D-tensors is depicted in Fig. 4(b), in which the z^{**} -axis of each D-tensor is chosen to be perpendicular to the Cu_3 plane. When the D-tensors are axial ($E = 0$), the tensors do not change (remain diagonal) upon rotation about their own z^{**} -axes, which are parallel to the z -axis.

Calculations of the EPR transitions were carried out using the EPR-NMR program kindly provided by Professor J. A. Weil of the University of Saskatchewan. The program not only allows setup of the spin Hamiltonian of three interacting spins with the desired g-tensor orientations and their zero-field splittings, but also finds the eigenvalues and eigenvectors through diagonalization of the Hamiltonian. To be consistent with our previous reports, the sign convention of the exchange interaction presented in this paper is opposite to the sign used in the program.

RESULTS AND DISCUSSION

EPR Signals Associated with the Oxidized C-clusters of pMMO

Nguyen et al.¹¹ were the first to report the 4.2 K EPR signal associated with the oxidized C-clusters in as-isolated pMMO membranes. We have recorded this spectrum again at 3 K on as-isolated pMMO-enriched membranes (pMMO content $\approx 80\%$ of total membrane proteins by weight) obtained by an improved method of culturing the *Methylococcus capsulatus* bacteria under controlled copper concentrations in growth medium.^{16,17} The pMMO in these membranes showed high specific activity whether NADH or duroquinol

was used to assay the propene epoxidation. When these pMMO-enriched membranes were solubilized in β -dodecyl-D-maltoside and purified by gel filtration, a pMMO-detergent complex of molecular mass 220 kDa was obtained, consisting of an $\alpha\beta\gamma$ protein monomer in a micelle of ~ 240 detergent molecules. The copper content of the pMMO thus purified contained ~ 14 atoms per protein monomer. Only adventitious iron was detected in the preparation ($Cu/Fe \approx 80:1$). The pMMO-detergent complex also showed excellent specific activity toward NADH or duroquinol when either of these reductants was employed as the co-substrate.¹⁷

The EPR spectrum of the as-isolated pMMO-enriched membranes is a composite of both a type 2 Cu(II) signal as well as a cluster Cu(II) signal, as shown in our companion paper.¹⁶ In the as-isolated pMMO, only the copper ions of the two C-clusters are presumably oxidized. According to the chemistry that we have proposed for the C-clusters,¹⁶ when the enzyme is turned over in dioxygen without the hydrocarbon co-substrate, one oxidized trinuclear Cu(II) cluster is formed at one of the C-cluster centers and a type 2 Cu(II) ion and an EPR silent bis(μ -oxo) Cu^{III}_2 or (μ - η^2 : η^2 -peroxo) Cu^{II}_2 dicopper core are formed at the other C-cluster site. Unlike EPR signals from type 1 or type 2 copper sites, the cluster signal could not be saturated even at relatively high microwave powers.¹¹

Fig. 5A depicts the 3 K EPR spectrum of the as-isolated pMMO at the low microwave power of $2 \mu W$.¹⁶ Under these conditions, neither the type 2 Cu(II) signal nor the cluster Cu(II) signal would be saturated. Accordingly, the putative cluster signal could be reliably obtained by recording the EPR of the as-isolated pMMO at this low microwave power and subtracting out a simulated spectrum of the type 2 Cu(II) associated with the other oxidized C-cluster, as was recently reported by us.¹⁶ Details of this deconvolution of the EPR spectrum of the C-clusters are as follows. Basically, the composite spectrum was taken as a linear combination of a type 2 Cu(II) signal and a trinuclear Cu(II) cluster signal (principal components). The type 2 signal was simulated from the g-values, the Cu(II) hyperfine tensor, and the ^{14}N superhyperfine interactions expected for tetragonal Cu(II) centers. The cluster signal was calculated by the method outlined in this study as described later. With the EPR parameters for the type 2 Cu(II) center held fixed, the various spin Hamiltonian parameters for the trinuclear Cu(II) cluster as well as the relative proportions of the two types of copper centers were then adjusted until a best fit was obtained between the simulated overall EPR spectrum and the experimental spectrum.

The deconvoluted spectra for the type 2 Cu(II) and the

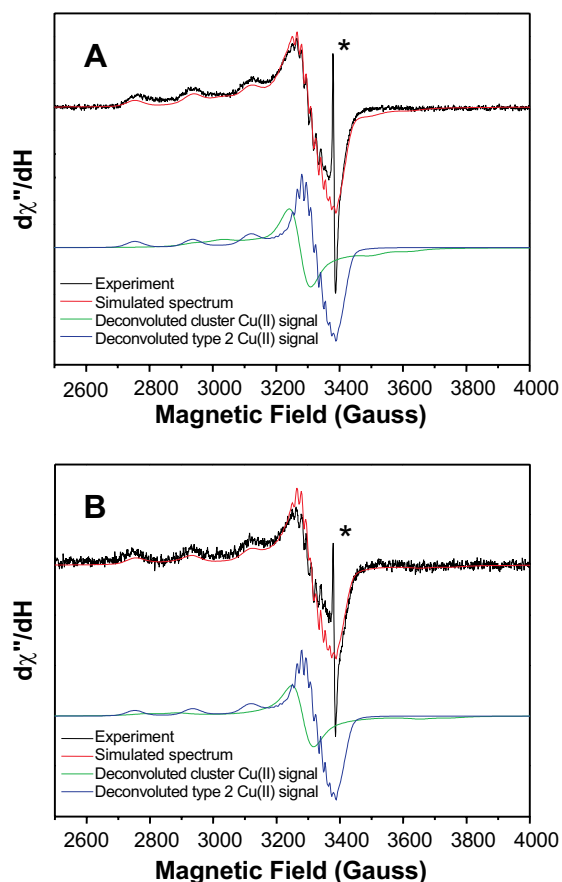


Fig. 5. The EPR spectra of as-isolated pMMO in highly pMMO-enriched membranes from *M. capsulatus* (Bath) recorded at X-band (9.49 GHz) under low microwave power levels at 3 K and 77 K (taken from reference 16), and those of the type 2 Cu(II) center and the putative oxidized C-cluster obtained from a deconvolution of the composite spectra. At each temperature, the composite spectrum was taken as a linear combination of a type 2 Cu(II) signal and a trinuclear Cu(II) cluster signal, and the relative proportions of the two signals as well as the spin Hamiltonian parameters for both the type 2 and the cluster centers were adjusted to best fit the observed composite spectrum. See reference 16 for details. **A:** Spectrum recorded at 3 K at the microwave power level of $2 \mu\text{W}$. **B:** Spectrum taken at 77 K at the microwave power level of $200 \mu\text{W}$. The simulated best-fit EPR spectra for the putative C-cluster were based on structural model **3** with g-tensors for the three Cu(II) ions of (1.983, 2.030, 2.218), (1.983, 2.029, 2.218) and (2.000, 2.033, 2.207); exchange interaction $J = +20 \text{ cm}^{-1}$, and zero-field splitting parameters $D = +0.017 \text{ cm}^{-1}$ (175 Gauss) and $E/D = 0.15$ at 3 K and $D = +0.019 \text{ cm}^{-1}$ (200 Gauss) and $E/D = 0.15$ at 77 K (green spectra).

cluster Cu(II) centers are delineated in Fig. 5A. Double integrations of the two component signals gave an intensity ratio of 0.9 ± 0.2 for the Cu(II) cluster to the type 2 Cu(II) signals. Spin counting of the composite EPR signal against CuSO_4 standards gave a total overall Cu(II) EPR intensity of 1.7 ± 0.4 copper ions per protein monomer.

Fig. 5B shows the corresponding EPR spectrum obtained for the oxidized trinuclear Cu(II) clusters at 77 K.¹⁶ This spectrum was recorded for the as-isolated pMMO at a sufficiently low microwave power ($200 \mu\text{W}$) where neither the type 2 Cu(II) signal nor the cluster Cu(II) signal would be saturated at this temperature. Again, we deconvoluted the observed spectrum into a sum of the type 2 and cluster Cu(II) signals, and their relative proportions were adjusted to fit the experimental spectrum. The identical spin Hamiltonian parameters for the type 2 and cluster signals that provided the best fit to the 3 K EPR spectrum were used at the outset to generate the two principal component spectra in the spectral deconvolution. It was only necessary to adjust slightly the zero-field splitting D for the Cu_3 cluster signal to obtain the best fit. At 77 K, however, the cluster signal needed to be corrected for the contributions from the excited doublet states (*vide infra*), even though it was still dominated by the transitions from the quartet state. These details are discussed later in this paper.

The deconvoluted type 2 and cluster Cu(II) signals are depicted in Fig. 5B. Double integrations of the two component signals that made up the 77 K EPR spectrum gave an intensity ratio of 0.8 ± 0.2 for the the cluster Cu(II) to the type 2 Cu(II) signals, and spin counting against CuSO_4 standards yielded a total EPR intensity for the composite spectrum corresponding to 1.6 ± 0.2 Cu(II) ion per protein molecule.

Assignment of the Putative C-Cluster EPR Spectrum

Fig. 6 depicts the energy levels for three exchange-coupled Cu(II) ions with a ferromagnetic ground state. It is relatively straightforward to assign the above relatively broad but nearly isotropic signal at $g \sim 2.1$ to the $S_T = 3/2$ quartet manifold of the trinuclear Cu(II) cluster. As described later, at 3 K only the quartet manifold contributes to the EPR, even for a relatively small J . However, depending on the magnitude of D , the three transitions within the quartet would contribute to the observed spectrum in varying proportions in different regions of the spectrum. For $|D| \ll g\beta H$, all three transitions contribute to give an isotropic feature centered at $g \sim 2.1$. As $|D|$ is gradually increased, the spectrum would still be dominated by this central feature. The resonance fields for the $-1/2 \rightarrow 1/2$ transition remain essentially isotro-

pic under these conditions. However, the resonance fields for the $-3/2 \rightarrow -1/2$ and $1/2 \rightarrow 3/2$ transitions become sensitive to $|D|$ and are anisotropic, appearing towards lower and higher fields of the central feature. The latter contributions could become part of the baseline for a powder sample because of the large orientational anisotropy of the resonance fields for these transitions when $|D|$ becomes sufficiently large. For $|D| > g\beta H$, the $-3/2 \rightarrow -1/2$ and $1/2 \rightarrow 3/2$ transitions would no longer be accessible by X-band EPR. Thus, only the $-1/2 \rightarrow 1/2$ transitions could be observed under these conditions, with the more intense perpendicular contributions resonating at $g \sim 4.2$ and the weaker parallel contribution at $g \sim 2.1$. Strains in the g , D , and E (if the cluster depart from equilateral symmetry) could also contribute to the breadth of the EPR spectrum and the smearing out of the transitions that add to the background.

Aside from their different intrinsic transition probabilities, the relative contributions of the three transitions to the composite spectrum depend also on the populations of the clusters occupying the various energy states of the quartet manifold. At 77 K, we also expect additional contributions to the cluster Cu(II) spectrum from the excited doublet states, if $|3J| \approx kT$ at this temperature. These various spectral features of a ferromagnetically coupled trinuclear Cu(II) cluster are high-

lighted in the detailed calculations summarized in the next section. Finally, there could be effects on the spectrum arising from thermal decoupling of the spins at the higher temperatures when the electron relaxation rate $1/T_1$ becomes sufficiently rapid compared with the exchange interactions among the Cu(II) spins. These latter considerations are complex and are beyond the scope of the present study.

Calculations of the Trinuclear-Copper-Cluster EPR at 3 K Based on Model Compounds

Here, we present the results of our efforts to simulate the EPR signal observed at 3 K for the oxidized trinuclear Cu(II) cluster of pMMO. Calculations on equilateral clusters will first be performed, and the local coordination geometry of the copper ions and their relative geometrical disposition within the cluster will be taken to be similar to that in model complexes **3** and **4**. Deviations from the symmetric triad will be then considered, including both the isosceles arrangement and the general triad. Although compound **6** is representative of an isosceles triangular model for a trinuclear cluster, some of our simulations were actually built on model complex **3** with the inclusion of a rhombic distortion in the zero-field splitting. The calculations will include variations over a range of zero-field splitting (D) in the case of equilateral

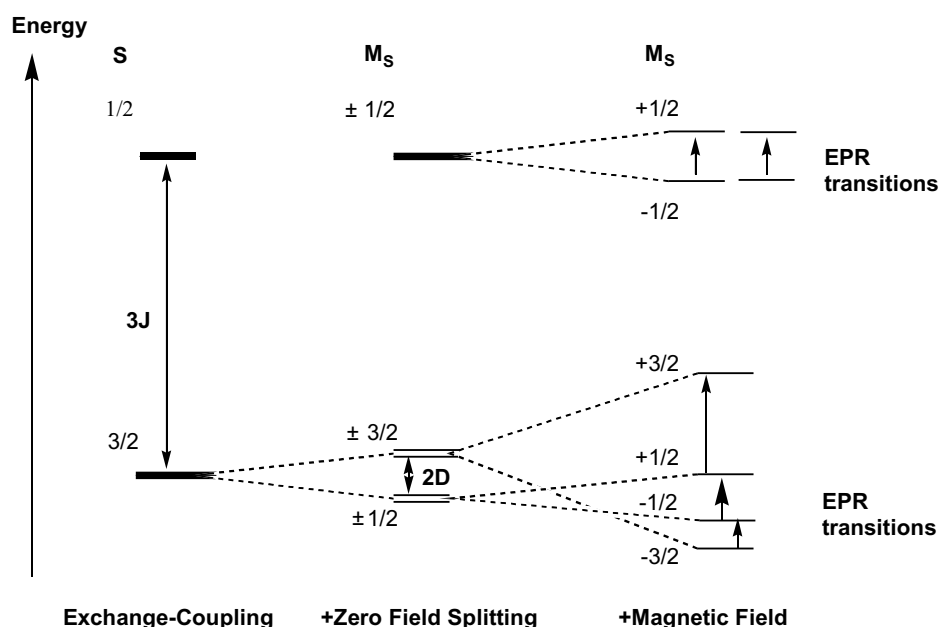


Fig. 6. Energy level diagram for a ferromagnetically coupled equilateral triad of Cu(II) ions (exchange interaction $J > 0$) with and without zero-field splitting ($D > 0$), and after the application of a magnetic field. When the triad deviates from equilateral, the degeneracy of the two upper doublet states is removed. The energy levels are otherwise unchanged. Only the EPR transitions observable at X-band are highlighted. For $J \approx 15\text{--}20\text{ cm}^{-1}$, only the quartet manifold is appreciably populated at 3 K. However, the transitions within the doublet states account for 16% of EPR intensity at 77 K. The spacings between the energy levels are not drawn to scale.

triad, but the effects of E, in addition to D, will also be explored in the case of the less symmetric clusters.

Equilateral Clusters

Fig. 7 summarizes the results of our EPR simulations of the putative cluster signal in pMMO for equilateral clusters. These calculations were performed using the g-tensor arrangements derived from the coordination geometry of **3** and **4** and a range for the spin Hamiltonian parameters (J and D) based on the estimates previously reported from the magnetization measurements.¹¹ From the temperature dependence of the magnetic moment and the magnetic susceptibility for the fully oxidized pMMO sample, Nguyen et al.¹¹ have deduced estimates of 15–20 cm⁻¹ and ≤ 0.05 cm⁻¹ (531 Gauss) for the exchange interaction J and the axial zero-field splitting D, respectively.

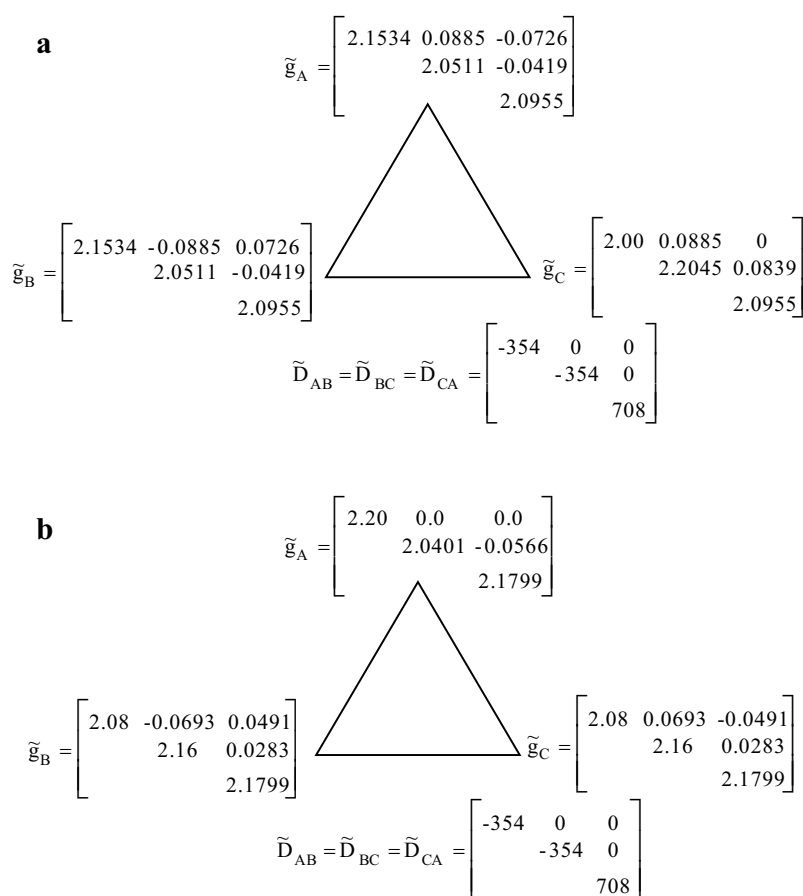
Scheme I lists the transformed local g-tensors ($\tilde{g}_{x,y,z}^*$) used for each of the three Cu(II) ions in the cluster and the interspin D-tensors between pairs of Cu(II) ions based on the

original sets reported for complexes **3** and **4**. Even though various g-values could be chosen to fit the EPR spectrum of the C-cluster, the degree of variation in the coordination geometry at the individual copper ions places a limit on the local g-tensor (diagonal in local coordinate system).

For a symmetric triad, $\tilde{D}_s = \frac{1}{6}(\tilde{D}_{AB} + \tilde{D}_{BC} + \tilde{D}_{CA})$. Since $D = 3/2 D_{||}$ or $3/2 D_{zz}$, for a D of 531 Gauss or 0.05 cm⁻¹, it follows then that $D_{||} = D_{zz} = 354$ Gauss. To yield a D = 531 Gauss in \tilde{D}_s , $D_{AB}^{zz} = D_{BC}^{zz} = D_{CA}^{zz} = 708$ Gauss so that $D_{||} = \frac{1}{6}(708 \times 3) = 354$ Gauss and $D = 3/2 D_{||} = 531$ Gauss. Since this D value represents an upper limit according to the magnetic susceptibility measurements, D was varied from 0 to 500 Gauss only in the EPR simulations summarized below.

Although we have assumed that the exchange coupling constant between pairs of Cu(II) ions in the cluster is 20 cm⁻¹, the outcome of the simulations is not sensitive to the exact value of J, so long as J is sufficiently large that the strong ex-

Scheme I The g-tensors for EPR simulations of pMMO based on the structures of **3** and **4** are shown in **a** and **b**, respectively. The D-tensors for the case of D = 531 G are also listed



change limit is obtained. For ferromagnetic coupling, the energy levels of the ground quartet state are insensitive to the magnitude of J within this limit.

In the strong exchange limit, only the transitions within the ground quartet states are thermally accessible at 3 K. In the presence of zero-field splitting, the details of the observed EPR signal are strongly dependent on the relative magnitude of the zero-field splitting and the frequency of the microwaves used to excite the spins in the spectrometer. When $g\beta H \gg D$, the spectrum is centered about $g \sim 2$, although the resonance fields for the $-3/2 \rightarrow -1/2$ and $1/2 \rightarrow 3/2$ transitions are not exactly coincident with the $-1/2 \rightarrow 1/2$ transition. As D becomes progressively larger in magnitude, the $-3/2 \rightarrow -1/2$ and $1/2 \rightarrow 3/2$ transitions begin to appear at higher and lower resonance fields. Variations of the trinuclear cluster EPR spectrum with axial zero-field splitting D from $D = 0$ through 500 Gauss are illustrated in Fig. 7 for the two equilateral representative coordination geometries noted earlier. The relative contributions of the three transitions to the composite spectrum of the quartet state are illustrated in Fig. 8. It is evident that for small D values, of the order of 50 Gauss, the $-3/2 \rightarrow -1/2$ and $1/2 \rightarrow 3/2$ transitions contribute mainly to the center of the EPR signal, resulting in an overall signal that remains relatively isotropic but with a larger resonance width. For a cluster with three Cu(II) ions with coordination geometry similar to that in the model complex **3**, the center of these EPR spectra can be readily explained by $\tilde{g}_{3/2,1}$ in eq 2, with an

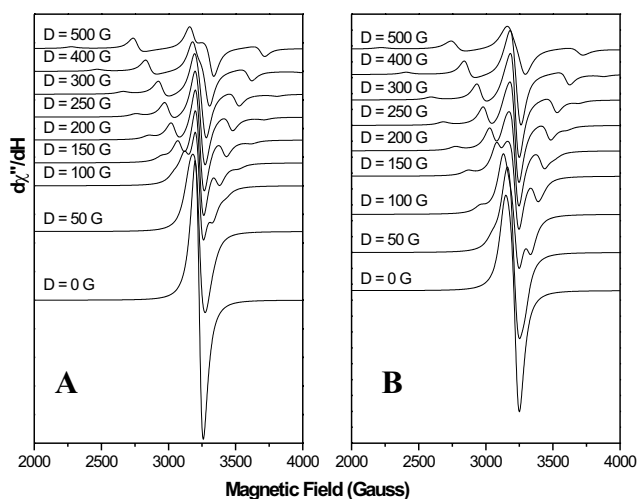


Fig. 7. Calculated 3 K EPR spectra for a ferromagnetic coupled trinuclear Cu(II) cluster for a range of the zero-field splitting D . Simulations shown in panels **A** and **B** are based on the equilateral structural model of compounds **3** and **4**, respectively. The g -tensors are listed in Scheme I.

effective g value corresponding to $g_{\text{avg}} \sim 2.1$ ($= 1/3 (\text{Tr } \tilde{g}^*)$). In the case of model **4**, all the composite spectra are shifted to somewhat lower fields, corresponding to the average g value of 2.14 for trigonal bipyramidal coordination.

Deviation from equilateral clusters

In general, there are three possibilities of the triangular arrangements for a trinuclear cluster: equilateral, isosceles, and the general triad. Since each spin interacts with the adjacent ones, the strength of these interactions determines the magnetic geometry of the triad. In the most general case when no two J_{ij} values are equal, then states with the same S_T value can be admixed, and the corresponding g -tensors are given by

$$\begin{aligned} \tilde{g}_{3/2,1} &= 1/3 (\tilde{g}_A + \tilde{g}_B + \tilde{g}_C), \\ \tilde{g}_{1/2,1} &= -(1/3 - 4/3 \sin^2 \lambda) \tilde{g}_A + 2(1/3 - 1/3 \sin^2 \lambda \\ &\quad - 1/\sqrt{3} \sin \lambda \cos \lambda) \tilde{g}_B + 2(1/3 - 1/3 \sin^2 \lambda \\ &\quad + 1/\sqrt{3} \sin \lambda \cos \lambda) \tilde{g}_C, \\ \tilde{g}_{1/2,0} &= (1 - 4/3 \sin^2 \lambda) \tilde{g}_A \\ &\quad + 2(1/3 \sin^2 \lambda + 1/\sqrt{3} \sin \lambda \cos \lambda) \tilde{g}_B \\ &\quad + 2(1/3 \sin^2 \lambda - 1/\sqrt{3} \sin \lambda \cos \lambda) \tilde{g}_C, \\ \lambda &= 1/2 \tan^{-1} [3^{1/2} (J_{AB} - J_{AC}) / (2J_{BC} - J_{AC} - J_{AB})]. \end{aligned} \quad (3)$$

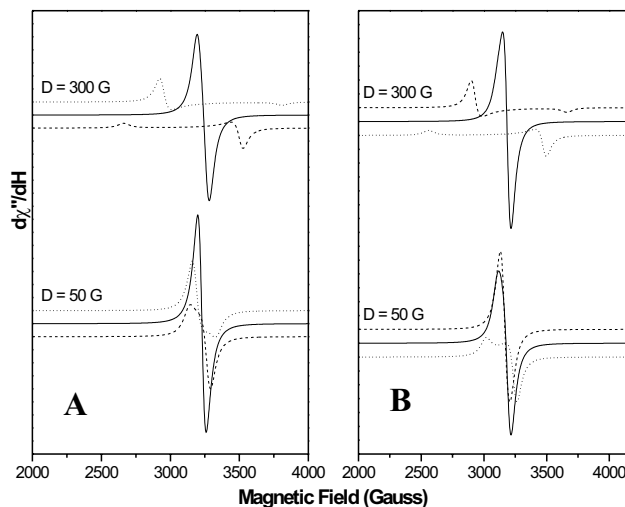


Fig. 8. Relative contributions of the three transitions to the composite spectrum of the quartet state. In each panel, dashed line, solid line, and dotted line represent the $-3/2 \rightarrow -1/2$, $-1/2 \rightarrow 1/2$, and $1/2 \rightarrow 3/2$ transitions, respectively. The simulations depicted in panels **A** and **B** are based on the structural model of compounds **3** and **4**, respectively. The g -tensors are listed in Scheme I. The individual spectra have not been weighted by the Boltzmann populations of the clusters among the spin states of the quartet.

Thus, the transitions within the two doublet states vary with the magnetic geometry of the triad. Note, however, that $\lambda = 0^\circ$ for both the equilateral and isosceles magnetic geometry, and the result for the symmetric triad is obtained.

Thus, for a ferromagnetically coupled trinuclear cluster in the strong exchange limit, when the observed EPR spectra are dominated by the transitions within the quartet states, with $g = \tilde{g}_{3/2,1}$, the observed g -values for the quartet do not vary with the shape of the triangle. The contributions from the two doublet states are also the same, except in the case of the totally asymmetric triad, but these transitions are only observed at rather elevated temperatures (depending on the magnitude of the exchange coupling).

Compound **6** is representative of an isosceles triangular model for the trinuclear clusters in pMMO. The local g -tensors ($g^*_{x,y,z}$) used for each of the three Cu(II) ions in the cluster and the inter-spin D -tensors between pairs of Cu(II) ions are listed in Scheme II. In this case, the exchange interactions between the terminal copper ions are negligible.^{32,44} Accordingly, both J_{BC} and D_{BC} were set to zero in the simulations. Spectral simulation results obtained with the axial zero-field splitting D varying from $D = 0$ through 500 Gauss are illustrated in Fig. 9A. Here, we find that the “central” feature in the spectrum is significantly more sensitive to D than those seen in Fig. 7, so that the spectrum exhibits greater anisotropy and weaker intensity. In Fig. 9B, the contribution of the three transitions within the quartet state are shown for $D = 50$ and 300 G. It is clear that the resonance fields for the $-3/2 \rightarrow -1/2$ and $1/2 \rightarrow 3/2$ transitions move away from the $g = 2$ region and manifest themselves towards higher and lower magnetic fields even for relatively smaller D 's, as compared to the case of the equilateral triangular clusters.

The general triad

As the triangular arrangement of a trinuclear cluster departs from the symmetric triad, the rhombic zero-field splitting becomes important. In order to ascertain the effects of the rhombic zero-field splitting parameter E on the EPR signal of the trinuclear Cu(II) cluster, non-zero E values were introduced in the EPR simulations of the cluster signal based on

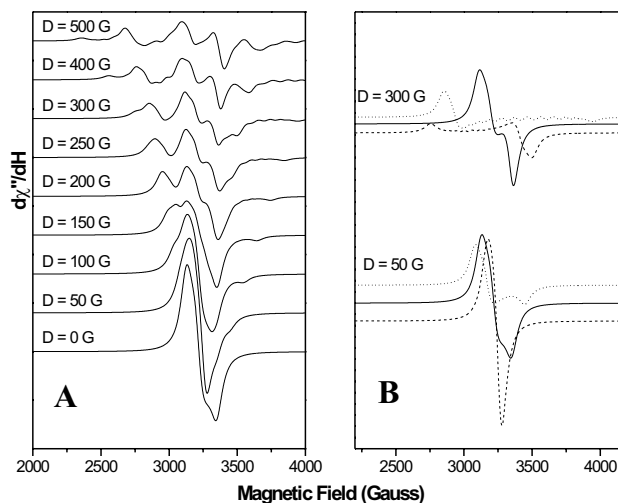


Fig. 9. **A.** Calculated 3 K EPR spectra for a ferromagnetically coupled trinuclear Cu(II) cluster based on the isosceles structural model of compound **6**. Details of the spin Hamiltonian are given in Scheme II. **B.** Contributions of the three transitions $-3/2 \rightarrow -1/2$ (dashed line), $-1/2 \rightarrow 1/2$ (solid line), and $1/2 \rightarrow 3/2$ (dotted line) within the quartet state are depicted separately in this panel. These component spectra have not been weighted by the Boltzmann populations among the spin states of the cluster.

Scheme II The g -tensors for EPR simulations of pMMO based on the structure of **6**. The D -tensors for the case of $D = 531$ G are also listed

$$\begin{array}{c}
 \tilde{g}_A = \begin{bmatrix} 2.025 & 0.0 & 0.025 \\ & 2.25 & 0.0 \\ & & 2.025 \end{bmatrix} \\
 \tilde{g}_B = \begin{bmatrix} 2.2393 & 0.0479 & 0.0054 \\ & 2.0357 & -0.0244 \\ & & 2.025 \end{bmatrix} \\
 \tilde{g}_C = \begin{bmatrix} 2.2393 & -0.0479 & 0.0054 \\ & 2.0357 & 0.0244 \\ & & 2.025 \end{bmatrix} \\
 \tilde{D}_{AB} = \tilde{D}_{CA} = \begin{bmatrix} -531 & 0 & 0 \\ & -531 & 0 \\ & & 1062 \end{bmatrix}; \tilde{D}_{BC} = 0
 \end{array}$$

the g -tensors of compound **6** (Scheme II). Some simulations are presented in Fig. 10 for the representative coordination geometries employed in this study, and varying D over the range of 50–500 Gauss, and E/D over the range of 0.01 to 0.3. As expected, the cluster spectra do not exhibit significant changes for small D values and small E/D 's. However, for sufficiently large D 's, the inclusion of a non-zero E leads to the smearing out of the features arising from $-3/2 \rightarrow -1/2$, and $1/2 \rightarrow 3/2$ transitions. The $-1/2 \rightarrow 1/2$ transition giving rise to the central feature of the spectra remains relatively unchanged even at relatively large D and E values, although the anisotropy of this signal is increased with increasing E .

Contributions from the excited doublet states

At sufficiently high temperatures (depending on the strength of the exchange coupling (J)), the two excited dou-

blet states become populated. Under these conditions, the transitions within the doublet states would contribute to the EPR spectrum of the trinuclear copper cluster. As mentioned in eq. 2, the g tensors associated with the transitions from the doublet states can be expressed as a linear combination of the local g -tensors of a symmetric triangular cluster. These g -tensors are normally not the same as that for the quartet states. As an example, we have calculated these transitions of the doublet states and compared their sub-spectra with those of the quartet state for the case of $D = 300$ G and $E = 0$. As shown in Fig. 11A, the EPR signals of the two doublets are centered at $g = 2.01$ and $g = 2.20$. Since the transition probability (double integration area) for each of these doublet contributions is 0.25, compared with 1.00 for the $-1/2 \rightarrow 1/2$ transition, and 0.75 for either the $-3/2 \rightarrow -1/2$ or the $1/2 \rightarrow 3/2$ transition, the bulk of the EPR intensity arises from the tran-

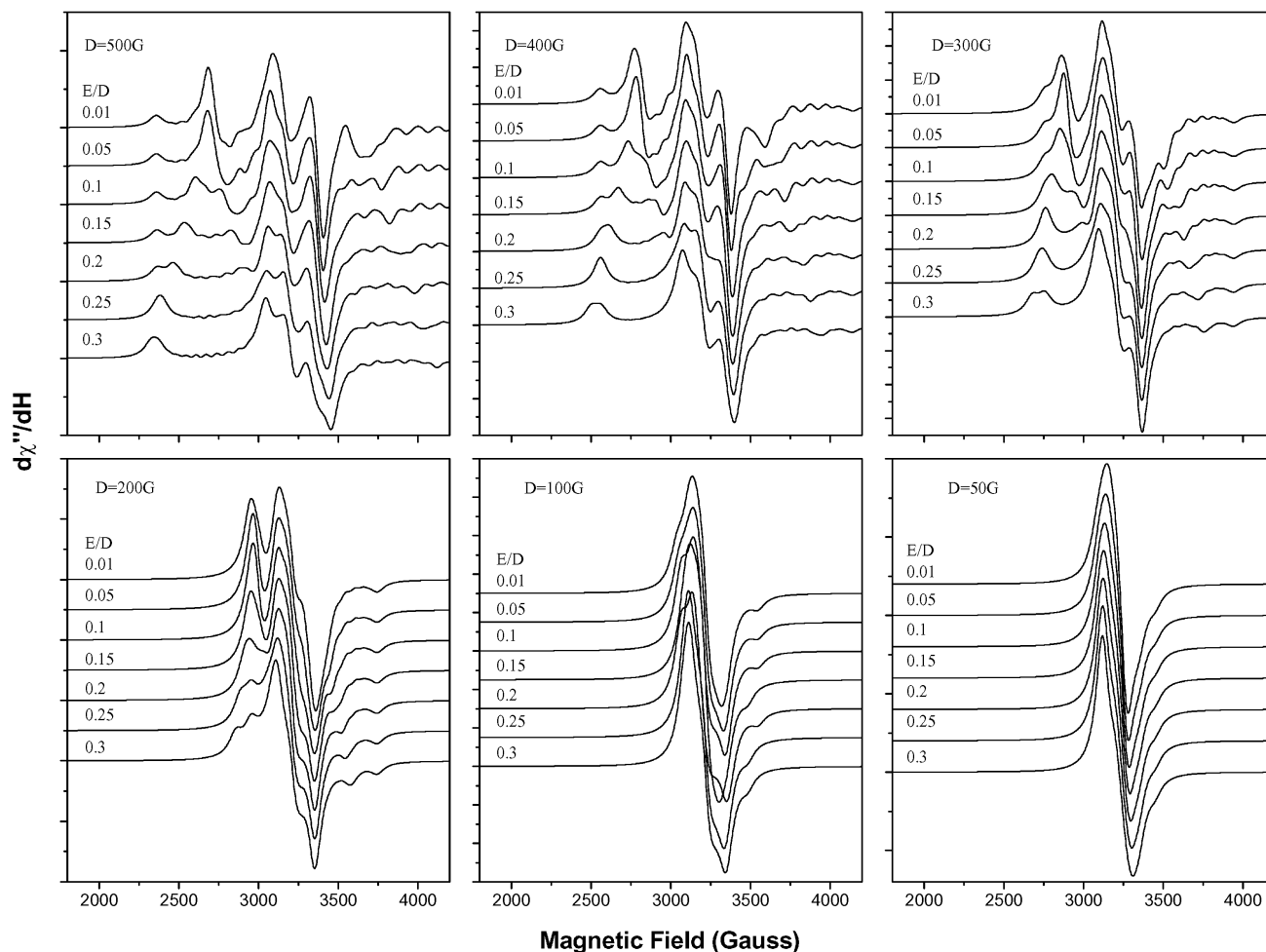


Fig. 10. The effects of a rhombic distortion in the zero-field splitting on the calculated 3 K EPR spectrum of a ferromagnetically coupled trinuclear Cu(II) cluster based on the isosceles structural model of compound **6** for different axial zero-field splittings ($50 \leq D \leq 500$ Gauss).

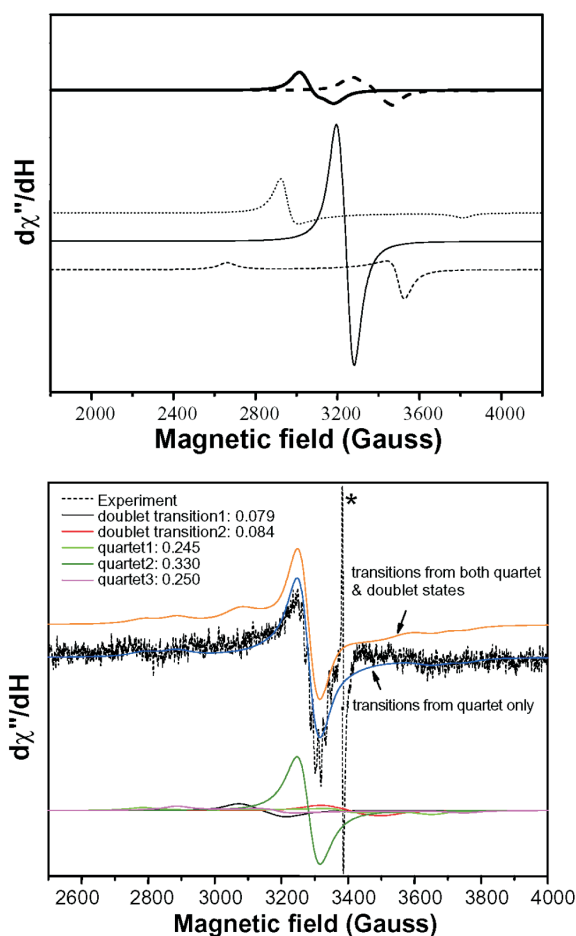


Fig. 11. **A.** Calculated EPR transitions for both the quartet ($-3/2 \rightarrow -1/2$ (dashed line), $-1/2 \rightarrow 1/2$ (solid line), and $1/2 \rightarrow 3/2$ (dotted line)) and the excited doublet states (heavy solid and dashed lines) based on the structural model of compound **3**, the spin Hamiltonian parameters $J = +20 \text{ cm}^{-1}$, $D = 250 \text{ Gauss}$, and $E/D = 0.15$, and the g -tensors listed in Scheme I. The spectra associated with the various transitions have not been weighted by the Boltzmann populations. **B.** Calculated overall composite EPR spectra for the putative cluster center at 77 K (weighted according to the Boltzmann populations) with and without the quartet state contributions, and comparison with the “observed” or deconvoluted “best fit” cluster EPR spectrum. Again, the simulations were based on the structural model of compound **3**, with $J = +20 \text{ cm}^{-1}$, $D = 250 \text{ Gauss}$, and $E/D = 0.15$, and the g tensors listed in Scheme I. The EPR signals calculated for the individual transitions (not weighted to Boltzmann population differences) are also depicted together with their relative weights in accordance with their expected transition probabilities.

sitions within the quartet state. Thus, in terms of integrated intensities, the contributions of the doublet states to the overall spectrum are relatively small, even when these states are appreciably populated. As noted earlier, the overall composite EPR spectrum is dominated by the central feature contributed by the $-1/2 \rightarrow 1/2$ transition of the quartet, as the intensities of the other two transitions of the quartet are spread out over a spectral width exceeding 1000 Gauss. As an illustration, we show at the bottom of Fig. 11B the overall EPR spectrum predicted for a trinuclear Cu(II) cluster at 77 K based on structural model **3**, the spin Hamiltonian parameters $J = +20 \text{ cm}^{-1}$, $D = 250 \text{ Gauss}$, and $E/D = 0.15$, and the g -tensors listed in Scheme I. The composite spectrum is clearly dominated by the $-1/2 \rightarrow 1/2$ transition of the quartet; however, a comparison of the simulated overall spectrum with and without the doublet contributions (orange spectrum *versus* blue spectrum) indicates that the latter contributions could stand out above the background in spite of their low integrated intensities. In contrast, the $-3/2 \rightarrow -1/2$ and $1/2 \rightarrow 3/2$ transitions of the quartet are expected to contribute primarily to the baseline.

Simulation of the 3 K EPR spectra for the putative C-cluster in pMMO

On the basis of these simulations, it is clear that the C-cluster signal from pMMO could be reproduced by an equilateral of three ferromagnetically coupled square pyramidal Cu(II) ions (model complex **3**) with an overall zero-field splitting of the order of $+0.017 \text{ cm}^{-1}$ (175 Gauss). For a zero-field splitting of this magnitude, all three transitions of the quartet manifold will contribute to the spectrum, even after weighting each contribution according to the Boltzmann population difference associated with the spin states involved in the transition of the cluster. With equilateral model complex **3**, the central feature appears at an overall g -value of 2.1, in excellent agreement with the observed spectrum. Note that this g -value for the cluster signal is significantly higher than g_{\perp} (~ 2.06) for the type 2 center (compare green and blue spectra in Fig. 5A).

The simulated 3 K spectrum for the putative C-cluster that provided the best fit to the overall composite spectrum obtained for the as-isolated pMMO at this temperature is shown in Fig. 5A. In order to improve the overall fit at the higher g -values, it was only necessary to introduce some asymmetry in the zero-field splitting (E). This spectrum was simulated with the following sets of g -values: (1.983, 2.030, 2.218), (1.983, 2.029, 2.218) and (2.000, 2.033, 2.207); and zero-field splitting parameters $D = +0.017 \text{ cm}^{-1}$ (175 gauss)

and $E/D = 0.15$. Thus, evidently, the cluster is essentially a symmetric cluster, or at most a slightly asymmetric triad.

A simple analysis based on the intrinsic transition probabilities of the three transitions and the Boltzmann population of the clusters at 3 K predicted an EPR intensity ratio 0.96 ± 0.1 for the putative cluster Cu(II) signal relative to that of a type 2 EPR center of the same concentration as the cluster (or 1/3 the copper concentration associated with the trinuclear cluster) at the same temperature. Thus, the observed ratio of 0.9 ± 0.2 corresponds essentially to the ratio of the cluster center to the type 2 center in the as-isolated pMMO. The total EPR intensity predicted for the composite signal observed at 3 K should then correspond to 1.9 ± 0.2 Cu(II) ions per protein, if there is indeed one type 2 Cu(II) center associated with the as-isolated pMMO. This predicted Cu(II) intensity is in good agreement with the value of 1.7 ± 0.4 determined from spin counting. Most precisely, these results indicate that the trinuclear Cu(II) cluster is contributing an intensity corresponding to 0.8 ± 0.3 of a Cu(II) ion to the EPR spectrum, and that 0.9 ± 0.3 of a type 2 Cu(II) center is being observed at 3 K. In other words, the composite EPR spectrum observed at 3 K is comprised of contributions from one type 2 Cu(II) center and one trinuclear Cu(II) center, within the experimental uncertainty of our EPR measurements.

As noted earlier, for a ferromagnetically coupled trinuclear Cu(II) cluster in the strong exchange limit, the observed EPR spectrum at 3 K is dominated by the transitions within the quartet states, and the observed g -values for the quartet are insensitive to the magnitude of the exchange interaction (provided J is sufficiently large), and do not vary with the shape of the triangle. On the other hand, the details of the spectrum are sensitive to the values of D and E .

The putative C-cluster EPR signal at 77 K

Depending on the magnitude of the exchange coupling, the two doublet states could contribute to the EPR spectrum at elevated temperatures. Under these circumstances, the contributions of the transitions from the two doublet states to the EPR intensity could be used to obtain a measure of the J coupling. The putative C-cluster signal that yielded the best fit to the observed composite EPR spectrum for the as-isolated pMMO at 77 K is shown in Fig. 5B. The spectrum was simulated using the same spin Hamiltonian parameters as used to best fit the 3 K spectrum, except that D was increased from 175 to 200 Gauss. The doublet state contributions were also included. The intensities of the doublet and quartet transitions were weighted according to the Boltzmann population of the clusters occupying these levels at 77 K assuming a J of

$+20 \text{ cm}^{-1}$. Under these conditions, the doublet state contributions would amount to some 16%, so that the cluster EPR intensity ratio would be substantially under-estimated if these excited state contributions were not taken into consideration in the simulation of the spectrum for the cluster Cu(II) center. Thus, the EPR intensity of the cluster signal relative to that of a type 2 center of 1/3 of the Cu(II) concentration at the same temperature allows one to obtain an estimate of the size of the exchange coupling. For a ferromagnetic exchange interaction of the magnitude of $J = +20 \text{ cm}^{-1}$, the total contribution of the cluster to the 77 K spectrum should correspond to 1.0 ± 0.1 isolated Cu(II) ions per protein at the same temperature. This is the intensity ratio expected for the cluster center relative to the type 2 center EPR signals in the deconvolution of the composite EPR spectrum for the as-isolated pMMO, if there is one type 2 Cu(II) center associated with the as-isolated enzyme. The measured intensity ratio is 0.8 ± 0.2 , and the measured total EPR intensity is 1.6 ± 0.2 Cu(II) ions per protein. These results indicate that the trinuclear Cu(II) cluster is contributing an intensity corresponding to 0.7 ± 0.2 of a Cu(II) ion to the EPR spectrum, and that 0.9 ± 0.2 of a type 2 Cu(II) center is being observed at this temperature.

Thus, the EPR intensity of the putative cluster signal, together with the difficulty in saturating this signal at high microwave powers, both point to the presence of a trinuclear Cu(II) center, in addition to a type 2 Cu(II) center in pMMO (of $\sim 1/3$ of the copper concentration per protein compared to the trinuclear copper cluster), when the enzyme is partially oxidized in the absence of hydrocarbon substrate.

SUMMARY

Toward understanding the nature of the ferromagnetically coupled trinuclear Cu(II) clusters in oxidized pMMO and the EPR spectra associated with these clusters, we have undertaken a review of the model triangular Cu(II) clusters that have been reported in the literature. Among the over 100-trinuclear copper clusters (including linear clusters) that have been synthesized and characterized so far, only a few show ferromagnetic exchange coupling. Nevertheless, these complexes exhibit sufficient variation in local ligand-coordination geometry and structural arrangements of the copper ions to allow us to build on these magneto-structural frameworks for the purpose of the present study. We found that it was possible to simulate the EPR observed for the putative C-cluster of pMMO on the basis of a slightly asymmetric triad of type 2 Cu(II) ions with an axial zero-field splitting of

$D = 0.017 \pm 0.002 \text{ cm}^{-1}$ (175 ± 25 Gauss). The variation in the EPR intensity of the cluster signal with temperature also provided an estimate of the exchange interaction of $15\text{--}20 \text{ cm}^{-1}$ between the copper ions, in accord with the estimate previously inferred from magnetic susceptibility data.

ACKNOWLEDGMENT

We thank Dr. Brian E. Schultz for numerous discussions on this work. We are indebted to Professor J. A. Weil, Department of Chemistry at University of Saskatchewan, Canada, who provided us with a copy of "Computer Program EPR-NMR", upon which much of this work is based. This work was supported by NIH grant GM22432 from the National Institute of General Medical Sciences, U.S. Public Health Service; and grants NSC 89-2113-M-001-021, 89-2113-M-001-098, 90-2113-M-001-006, 90-2113-M-001-080 and 91-2113-M-006-006 from the National Science Council of the Republic of China.

Received May 5, 2004.

REFERENCES

- Allendorf, M. D.; Spira, D. J.; Solomon, E. I. *Proc. Natl. Acad. Sci. USA* **1985**, *82*, 3063.
- Cole, J. L.; Clark, P. A.; Solomon, E. I. *J. Am. Chem. Soc.* **1990**, *112*, 9534.
- Cole, J. L.; Tan, G. O.; Yang, E. K.; Hodgson, K. O.; Solomon, E. I. *J. Am. Chem. Soc.* **1990**, *112*, 2243.
- Sundaram, U. M.; Zhang, H. H.; Hedman, B.; Hodgson, K. O.; Solomon, E. I. *J. Am. Chem. Soc.* **1997**, *119*, 12525.
- Zaitseva, I.; Zaitsev, V.; Card, G.; Moshkov, K.; Bax, B.; Ralph, A.; Lindley, P. *J. Bioinorg. Chem.* **1996**, *1*, 15.
- Messerschmidt, A.; Ladenstein, R.; Huber, R.; Bolognesi, M.; Avigliano, L.; Petruzzelli, R.; Rossi, A.; Finazziagro, A. *J. Mol. Biol.* **1992**, *224*, 179.
- Messerschmidt, A.; Luecke, H.; Huber, R. *J. Mol. Biol.* **1993**, *230*, 997.
- Solomon, E. I.; Sundaram, U. M.; Machonkin, T. E. *Chem. Rev.* **1996**, *96*, 2563.
- Blackburn, N. J. In *Bioinorganic Chemistry of Copper*; Karlin, K. D.; Tyeklár, Z., Ed.; Chapman & Hall: New York, 1993; pp 164-183.
- Eipper, B. A.; Quon, A. S. W.; Mains, R. E.; Boswell, J. S.; Blackburn, N. J. *Biochemistry* **1995**, *34*, 2857.
- Nguyen, H.-H. T.; Shiemke, A. K.; Jacobs, S. J.; Hales, B. J.; Lidstrom, M. E.; Chan, S. I. *J. Biol. Chem.* **1994**, *269*, 14995.
- Nguyen, H.-H. T.; Nakagawa, K. H.; Hedman, B.; Elliott, S. J.; Lidstrom, M. E.; Hodgson, K. O.; Chan, S. I. *J. Am. Chem. Soc.* **1996**, *118*, 12766.
- Nguyen, H.-H.; Elliott, S. J.; Yip, J. H.; Chan, S. I. *J. Biol. Chem.* **1998**, *273*, 7957.
- Elliott, S.-J.; Zhu, M.; Tso, L.; Nguyen, H.-H. T.; Yip, J.-H. K.; Chan, S. I. *J. Am. Chem. Soc.* **1997**, *119*, 9949.
- Yu, S. S.-F.; Wu, L.-Y.; Chen, K. H.-C.; Luo, W.-I.; Huang, D.-S.; Chan, S. I. *J. Biol. Chem.* **2003**, *278*, 40658.
- Chen, K. H.-C.; Chen, C.-L.; Tseng, C.-F.; Yu, S. S.-F.; Ke, S.-C.; Lee, J.-F.; Nguyen, H.-H. T.; Elliott, S. J.; Alben, J. O.; Chan, S. I. *J. Chin. Chem. Soc.* **2004**, *51*, 1081.
- Yu, S. S.-F.; Chen, K. H.-C.; Tseng, M. Y.-H.; Wang, Y.-S.; Tseng, C.-F.; Chen, Y.-J.; Huang, D.-S.; Chan, S. I. *J. Bacteriol.* **2003**, *185*, 5915.
- Kahn, O. *Angew. Chem. Int. Ed. Engl.* **1985**, *24*, 834.
- Miller, J. S.; Epstein, A. J. *Angew. Chem. Int. Ed. Engl.* **1994**, *33*, 385.
- Stumpf, H. O.; Ouahab, L.; Pei, Y.; Bergerat, P.; Kahn, O. *J. Am. Chem. Soc.* **1994**, *116*, 3866.
- Beckett, R.; Hoskins, B. F. *J. Chem. Soc., Dalton Trans.* **1972**, 291.
- Baral, S.; Chakravorty, A. *Inorg. Chim. Acta* **1980**, *39*, 1.
- Butcher, R. J.; O'Connor, C. J.; Sinn, E. *Inorg. Chem.* **1981**, *20*, 537.
- Hulsbergen, F. B.; Hoedt, R. W. M.; Verschoor, G. C.; Reedijk, J.; Spek, A. L. *J. Chem. Soc., Dalton Trans.* **1983**, 539.
- Comarmond, J.; Dietrich, B.; Lehn, J. M. R. L. *J. Chem. Soc., Chem. Commun.* **1985**, 74.
- Costes, J. P.; Dahan, F.; Laurent, J. P. *Inorg. Chem.* **1986**, *25*, 413.
- Kwiatkowski, M.; Kwiatkowski, E.; Olechnowicz, A.; Ho, D. M.; Deutsch, E. *Inorg. Chim. Acta.* **1988**, *150*, 65.
- Agnus, Y.; Louis, R.; Metz, B.; Boudon, C.; Gisselbrecht, J. P.; Gross, M. *Inorg. Chem.* **1991**, *30*, 3155.
- Chaudhuri, P.; Winter, M.; DellaVedova, B. P. C.; Bill, E.; Trautwein, A.; Gehring, S.; Fleischhauer, P.; Nuber, B.; Weiss, J. *Inorg. Chem.* **1991**, *30*, 2148.
- Chaudhuri, P.; Karpenstein, I.; Winter, M.; Butzlaff, C.; Bill, E.; Trautwein, A. X.; Florke, U.; Haupt, H. J. *J. Chem. Soc., Chem. Commun.* **1992**, 321.
- Adams, H.; Bailey, N. A.; Dwyer, M. J. S.; Fenton, D. E.; Hellier, P. C.; Hempstead, P. D.; Latour, J. M. *J. Chem. Soc., Dalton Trans.* **1993**, 1207.
- Gehring, S.; Fleischhauer, P.; Paulus, H.; Haase, W. *Inorg. Chem.* **1993**, *32*, 54.
- Meenakumari, S.; Tiwary, S. K.; Chakravarty, A. R. *Inorg. Chem.* **1994**, *33*, 2085.
- Cole, A.; Root, D.; Mukherjee, P.; Solomon, E.; Stack, T. *Science* **1996**, *273*, 1848.
- Spiccia, L.; Graham, B.; Hearn, M. T. W.; Lazarev, G.;

- Moubaraki, B.; Murray, K. S.; Tiekink, E. R. T. *J. Chem. Soc., Dalton Trans.* **1997**, 4089.
36. Suh, M. P.; Han, M. Y.; Lee, J. H.; Min, K. S.; Hyeon, C. *J. Am. Chem. Soc.* **1998**, *120*, 3819.
37. Bernhardt, P. V.; Sharpe, P. C. *J. Chem. Soc., Dalton Trans.* **1998**, 1087.
38. Kodera, M.; Tachi, Y.; Kita, T.; Kobushi, H.; Sumi, Y.; Kano, K.; Shiro, M.; Koikawa, M.; Tokii, T.; Ohba, M.; Okawa, H. *Inorg. Chem.* **2000**, *39*, 226.
39. Kolks, G.; Lippard, S. J.; Waszczak, J. V. *J. Am. Chem. Soc.* **1980**, *102*, 4832.
40. Escuer, A.; Vicente, R.; Penalba, E.; Solans, X.; Fonte, B. M. *Inorg. Chem.* **1996**, *35*, 248.
41. Springborg, J.; Glerup, J.; Sotofte, I. *Acta Chem. Scand.* **1997**, *51*, 832.
42. Bazzicalupi, C.; Bencini, A.; Bencini, A.; Bianchi, A.; Corana, F.; Fusi, V.; Giorgi, C.; Paoli, P.; Paoletti, P.; Valtancoli, B.; Zanchini, C. *Inorg. Chem.* **1996**, *35*, 5540.
43. Girard, J. J.; Charlot, M. F.; Kahn, O. *Mol. Phys.* **1977**, *34*, 1063.
44. Fleischhauer, P.; Gehring, S.; Saal, C.; Haase, W.; Tomkowicz, Z.; Zanchini, C.; Gatteschi, D.; Davidov, D.; Barra, A. L. *J. Magn. Magn. Mater.* **1996**, *159*, 166.
45. Ruiz, E.; Alemany, P.; Alvarez, S.; Cano, J. *J. Am. Soc. Chem.* **1997**, *119*, 1297.
46. Bencini, A.; Gatteschi, D. In *EPR of Exchange-coupled Systems*; Springer: Berlin, 1990.